Proc. Estonian Acad. Sci. Eng., 2006, **12**, 3-1, 176–187

Erosion-corrosion of Cr_3C_2-Ni cermets in salt water

Maksim Antonov[a], Margaret Stack[b] and Irina Hussainova[a]

[a] Department of Materials Engineering, Tallinn University of Technology, Ehitajate tee 5, 19086 Tallinn, Estonia; maksim.antonov@ttu.ee, irhus@staff.ttu.ee

b Department of Mechanical Engineering, University of Strathclyde, James Weir Building, Montrose St. 75, Glasgow G1 1XJ, UK; margaret.stack@strath.ac.uk

Received 24 October 2005, in revised form 6 March 2006

Abstract. Chromium carbide based cermets are popular materials in different industrial applications due to their unique properties. These materials have outstanding erosion resistance up to 1000 °C and excellent oxidation resistance up to 850 °C. Their corrosion resistance in different corroding mediums is favorably higher than that of conventional WC hard metals or stainless steel. These materials can be applied as coatings with properties comparable to bulk materials. In this work different regimes with prevailing role of erosion or corrosion processes were found. Erosion-corrosion maps for material selection were constructed and discussed. The weight loss of the samples during simultaneous effect of corrosion and wear processes was found to be complicated and cannot be evaluated as simple summation of these two processes. SEM study of material surfaces before and after erosion-corrosion tests were conducted and the prevailing mechanisms of the material behaviour were evaluated.

Key words: chromium carbide, cermet, erosion-corrosion, mapping, synergistic effect, pH.

1. INTRODUCTION

Chromium carbide (Cr_3C_2, Cr_7C_3 and others) based cermets are materials of interest in different application areas due to their unique properties. Nickel or nickel based alloys are usually applied as the matrix. These materials have outstanding erosion resistance at least up to 1000 °C and excellent oxidation resistance up to 850 °C [1]. Their corrosion resistance in different corroding mediums is higher than that of conventional WC hard metals or stainless steel [2]. These materials can be applied as coatings with properties comparable to bulk materials. Coatings can be deposited without binder which further increases the corrosion resistance [3,4].

The wastage of materials in erosion-corrosion conditions is a function of a large number of variables: target material properties (i.e. composition, hardness, tough-

ness and elastic modulus), abrasive particle characteristics (hardness, angularity), test conditions (impact angle, velocity, particles mass and concentration), and corrosive media (flow viscosity, pH, electrochemical potential, temperature, pressure and presence of ions such as Cl^-) [5]. The significant difference in erosion and corrosion properties of the constituents of cermets is also one of the important factors that control the erosion-corrosion process. Therefore it is of interest to apply a methodology that allows to analyse independent contributors of erosion and corrosion processes, their interaction, regimes and criteria for such regime transitions.

Test methods for the study of the wear-corrosion synergism usually utilize measurement of the material loss under wear conditions with and without corrosion or under corrosion conditions with and without wear. Faraday's second law is an important tool that links the degradation due to corrosion [6]. The methodology given in [5] also describes the mapping technique for presenting the results and is applied as the basis in the present work. Mapping techniques are increasingly being used for presenting tribo-corrosion mechanisms for optimization of material and process parameters selection by specialists in different industrial areas [7–9].

The main aim of this work was to apply the testing and calculation techniques to evaluate the erosion and corrosion properties of chromium carbide cermets as individual processes and their interaction at room temperature.

2. EXPERIMENTAL

The test apparatus used in this study was similar to that proposed by Zu [10]. The principal scheme is shown in Fig. 1.

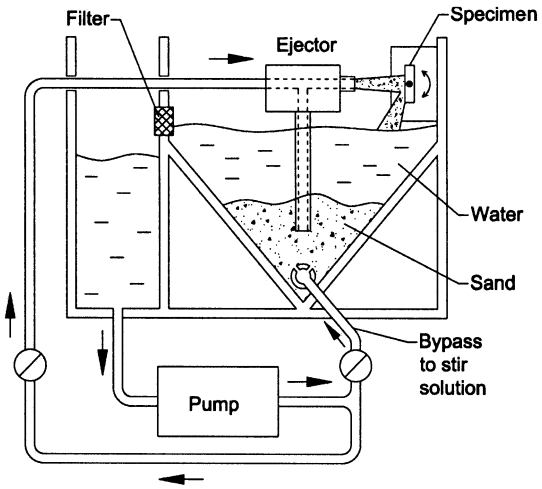

Fig. 1. Principal scheme of the erosion-corrosion test rig.

A plastic tank is used as a chamber. The solution is delivered with high pressure to the ejector where it produces a partial vacuum due to the venturi effect. Thus, the slurry underneath the tube could be mixed with the flowing solution by means of suction. The pump with adjustable capacity and a system of valves was used to adjust the required velocity of solution. By changing the ejector parameters it is also possible to change the concentration of particles in solution.

The typical three-electrode system was incorporated into the test rig to enable *in situ* electrochemical tests to be made and to control the potential of the specimen. A saturated calomel electrode (SCE) was used as a reference electrode. Graphite was used as auxiliary electrode. All potentials reported are with respect to SCE throughout this work. Electrochemical measurements were made using the GILL AC potentiostat of ACM Instruments, controllable by PC.

Testing conditions and mechanical properties of materials tested are presented in Tables 1 and 2, respectively. Testing conditions were similar to the conditions applied in previous works to provide a basis for comparison of erosion-corrosion response of different materials [5]. The mean size of the carbide grains was in the range of 2–5 μm for all cermets investigated. The surface of the specimens was polished with 1 μm diamond suspension.

The Stereoscan 360 (Leica Cambridge Instruments, Cambridge, UK, 1975) Scanning Electron Microscope was employed for the investigation of degradation mechanisms during erosion-corrosion. SEM imaging presented in the current work was conducted by secondary electrons at 20 kV accelerating voltage and beam current of 100 nA.

Table 1. Testing conditions

Parameter	Description
Abrasive	Silica sand with mean size of 0.1 mm
Solution	Artificial sea water with pH of 8.2, prepared according to ASTM 1141-98
Impact velocity	4 m s^{-1}
Impact angle	90°
Concentration of abrasive in solution	8% by weight
Potentials	−600 (cathodic protection), 0, +250, +500 mV

Table 2. Mechanical properties of materials tested

Grade	Ni content, wt%*	Vickers hardness, HV	Fracture toughness K_{IC}, MPa $m^{0.5}$
C10	10	1490	9.5
C20	20	1368	13.8
C40	40	900	19.0

* The rest is Cr_3C_2.

3. RESULTS AND DISCUSSION

Polarization curves were generated by applying potentials from −1000 to +1000 mV at the sweep rate of 1 mV s^{-1} during the impact of abrasive particles and without particles in the solution. Results are presented in Figs. 2 and 3.

It can be seen that the corrosion potential (E_{corr}) depends neither on material composition nor on properties of the abrasive particles and is −200 mV with reference to SCE. The corrosion current of cermet grades with higher binder content was higher. The passivity regions for C10 and C20, tested without abrasive particles, were found at potentials above 750 mV. The tests in the presence of abrasive particles has shown the shift of passivity regions to the higher potentials.

The wastage was defined as follows [5]:

$$K_{ec} = K_e + K_c, \tag{1}$$

where K_e is the total erosion rate, K_c is the total corrosion rate and K_{ec} is the overall erosion-corrosion rate.

$$K_e = K_{eo} + \Delta K_e, \tag{2}$$

$$K_c = K_{co} + \Delta K_c, \tag{3}$$

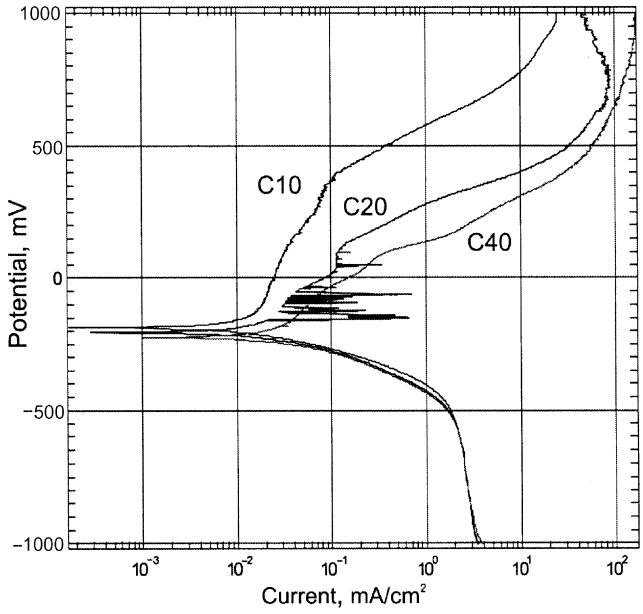

Fig. 2. Tafel slopes for materials tested in the presence of abrasive particles.

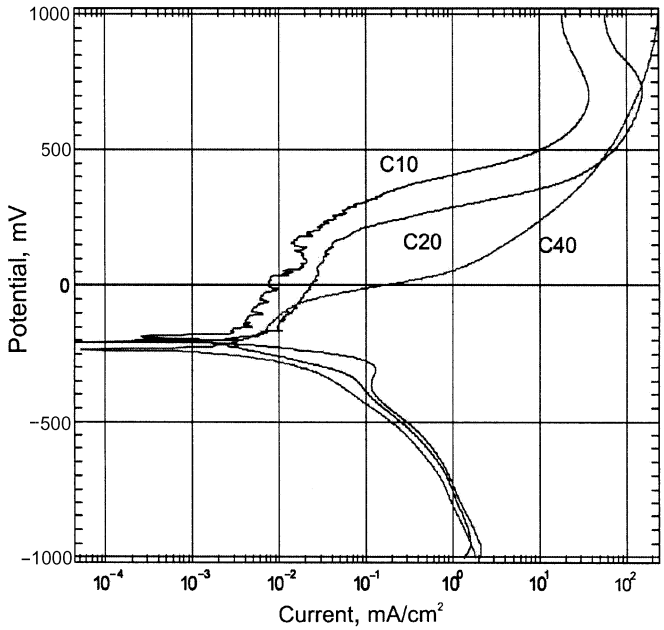

Fig. 3. Tafel slopes for materials tested without abrasive particles.

where K_{eo} is the erosion rate in the absence of corrosion, ΔK_e is the effect of corrosion on the erosion rate, K_{co} is the corrosion rate in the absence of erosion, and ΔK_c is the effect of erosion on the corrosion rate.

Erosion-corrosion regimes can be defined as follows:

$$\frac{K_e}{K_c} < 0.1 \quad \text{corrosion}$$

$$0.1 \le \frac{K_e}{K_c} < 1 \quad \text{corrosion-erosion}$$

$$1 \le \frac{K_e}{K_c} < 10 \quad \text{erosion-corrosion}$$

$$\frac{K_e}{K_c} \ge 10 \quad \text{erosion}$$

Data, concerning the transition between erosion-corrosion regimes, is presented in Table 3 and in Fig. 4.

It is not surprising that at low potentials and under cathodic protection the main wastage mechanism is erosion. At higher potentials the corrosion rate becomes comparable to that of erosion. The erosion rate is greater than corrosion rate for cermets with lower binder content.

Table 3. Values of K_{ec}, K_e, K_c and K_e/K_c for the construction of erosion-corrosion regime and wastage maps of Cr_3C_2-Ni cermets

Grade	Potential, mV	K_{ec}, mg h^{-1} cm^{-2}	K_{ec}, mg kg^{-1} cm^{-2}	K_e, mg h^{-1} cm^{-2}	K_c, mg h^{-1} cm^{-2}	K_e/K_c
C10	−600	0.13	0.003	0.13	0.00	–
C10	0	0.52	0.011	0.51	0.01	50.9
C10	+250	0.52	0.011	0.43	0.09	4.9
C10	+500	7.75	0.163	5.59	2.16	2.6
C20	−600	0.52	0.011	0.52	0.00	–
C20	0	0.52	0.011	0.49	0.03	18.5
C20	+250	3.72	0.078	2.59	1.13	2.3
C20	+500	42.43	0.895	32.80	9.63	3.4
C40	−600	0.60	0.013	0.60	0.00	–
C40	0	1.04	0.022	0.96	0.08	12.6
C40	+250	32.39	0.683	24.56	7.83	3.1
C40	+500	80.33	1.695	57.98	22.35	2.6

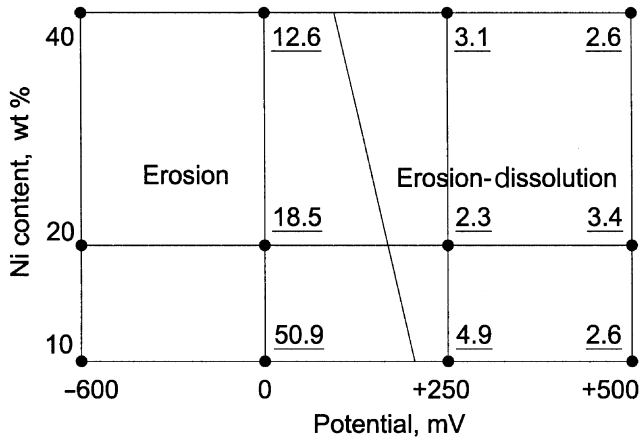

Fig. 4. Erosion-corrosion regime map. Underlined numbers are values of K_e/K_c.

An erosion-corrosion wastage map (Fig. 5) was constructed to chart the difference between levels of wastage (K_{ec}) as a function of binder content and electrochemical potential. The areas “low”, “medium” and “high” correspond to K_{ec} values less than or equal to 0.01 mg kg^{-1} cm^{-2}, between 0.01 and 0.1 mg kg^{-1} cm^{-2}, and greater or equal to 0.1 mg kg^{-1} cm^{-2}, respectively.

Corrosion may enhance erosion through preferential dissolution of the matrix material, through assisting the micro-cracking process in materials prone to stress corrosion cracking or through formation of porous layers of corrosion products, which are easily removed between erosion “events”. This “synergistic” effect may lead to very high wastage rates, and thus is important to predict and characterize erosion.

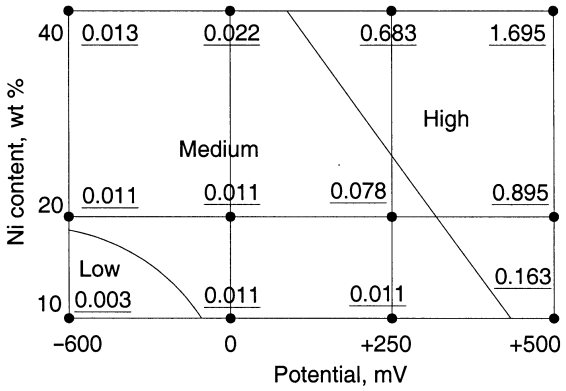

Fig. 5. Erosion-corrosion wastage map of Cr_3C_2-Ni. Underlined numbers are values of K_{ec}.

For synergistic effects, the following regime definitions apply:

$$\frac{\Delta K_e}{K_{eo}} < 1 \quad \text{low synergistic effect}$$

$$1 \le \frac{\Delta K_e}{K_{eo}} < 10 \quad \text{medium synergistic effect}$$

$$\frac{\Delta K_e}{K_{eo}} \ge 10 \quad \text{high synergistic effect}$$

Table 4 gives the parameters needed for the map construction. The erosion-corrosion maps show the transition between different rates of synergistic effect for chromium carbide based cermets. Figure 6 presents a materials performance

Table 4. Values of ΔK_e, K_{eo}, ΔK_c, K_{co}, $\Delta K_e/K_{eo}$ and $\Delta K_c/K_{co}$ for the construction of maps showing transition between different synergistic and additive regimes of Cr_3C_2-Ni cermets

Grade	Potential, mV	ΔK_e, mg h^{-1} cm^{-2}	K_{eo}, mg h^{-1} cm^{-2}	ΔK_c, mg h^{-1} cm^{-2}	K_{co}, mg h^{-1} cm^{-2}	$\Delta K_e/K_{eo}$	$\Delta K_c/K_{co}$
C10	−600	0.00	0.13	0.00	0.00	–	–
C10	0	0.38	0.13	0.01	<<0.01	2.9	2521.8
C10	+250	0.30	0.13	0.08	0.01	2.3	9.9
C10	+500	5.46	0.13	1.44	0.71	42.0	2.0
C20	−600	0.00	0.52	0.00	0.00	–	–
C20	0	−0.03	0.52	0.03	<<0.01	−0.1	85.3
C20	+250	2.07	0.52	0.47	0.65	4.0	0.7
C20	+500	32.28	0.52	5.48	4.15	62.1	1.3
C40	−600	0.00	0.60	0.00	0.00	–	–
C40	0	0.36	0.60	−0.09	0.17	0.6	−0.6
C40	+250	23.96	0.60	2.05	5.78	39.9	0.4
C40	+500	57.38	0.60	7.02	15.33	95.6	0.5

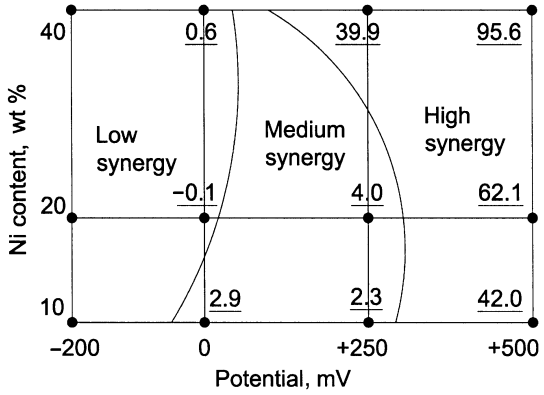

Fig. 6. Erosion-corrosion map showing the transition between different synergistic regimes for Cr_3C_2-Ni. Underlined numbers are values of $\Delta K_e / K_{eo}$.

map as a function of matrix content and potential. Increase in potential results in increase of synergistic effect.

Erosion can enhance corrosion through removal of the protective film on the surface. This is the so-called "additive" effect [11]. The following regimes can be used to define regimes of additive behaviour:

$$\frac{\Delta K_c}{K_{co}} < 1 \quad \text{low additive effect}$$

$$1 \le \frac{\Delta K_c}{K_{co}} < 10 \quad \text{medium additive effect}$$

$$\frac{\Delta K_c}{K_{co}} \ge 10 \quad \text{high additive effect}$$

The erosion-corrosion map showing the transition between different rates of additive effect for chromium carbide based cermets is presented in Fig. 7. Increases in Ni binder content and potential lead to lower values that describe additive effect. However, it is found to be correct only for materials with low binder content (10 and 20wt% of Ni). The grade with 40% of Ni matrix seems to be almost not affected by the change in the potential.

Scanning electron microscope study of material surfaces before and after erosion–corrosion tests was conducted to find the prevailing mechanism of material removal. Nickel corrosion products with the shape of islands of maximum dimension of 15 mm were found at the surface of C10 cermet (Fig. 8). The number of islands at the surface of C20 was at least 10 times less. Almost no corrosion products were found at the surface of material with the highest binder content C40 (Fig. 9). Corrosion starts in the centre of the biggest binder accumulation and develops towards the grain boundaries and inside the material (see scheme in Fig. 10).

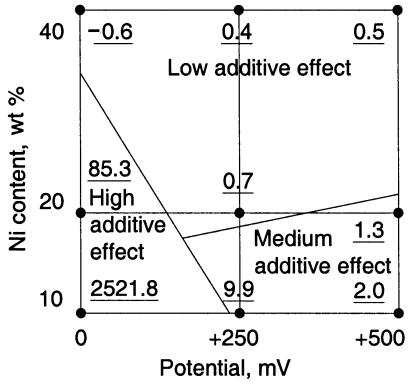

Fig. 7. Erosion-corrosion map showing the transition between different additive regimes for Cr_3C_2-Ni. Underlined numbers are values of $\Delta K_c / K_{co}$.

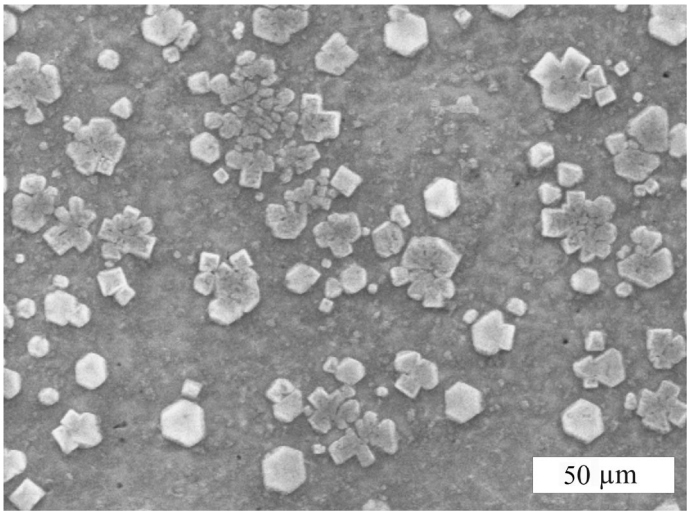

Fig. 8. SEM micrograph of Cr_3C_2-Ni cermet with 10 Ni wt % after erosion-corrosion test at potential of +500 mV. White islands indicate corrosion products.

The importance of surface layers by protection against corrosion and erosion was emphasized elsewhere [12,13]. According to SEM micrographs it is possible to conclude that the protective properties of corrosion islands could be established only in case of cermets with a low binder content. The formation of an overall protective layer is not possible due to the low adhesion between the chromium carbides and corrosion products. Besides, the layer of brittle corrosion products attached to the stiff carbide grain is easily removed due to the inability of the layer to absorb energy through deformation. The maximum size of corrosion products depends directly on the free surface of the binder phase in the area of

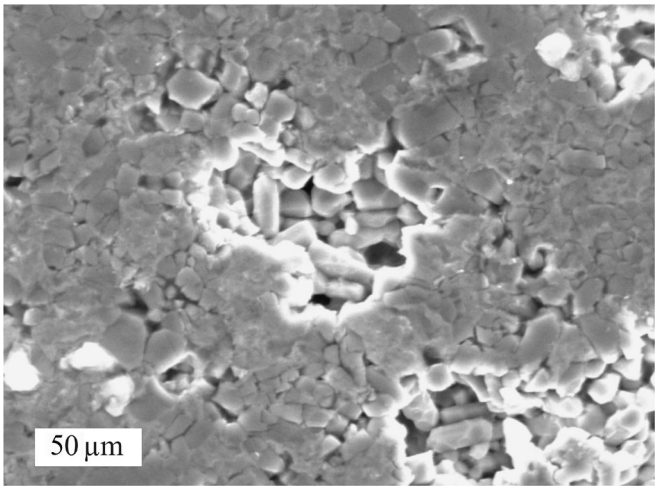

Fig. 9. SEM micrograph of Cr_3C_2-Ni cermet with 40 Ni wt % after erosion-corrosion test at potential of +500 mV.

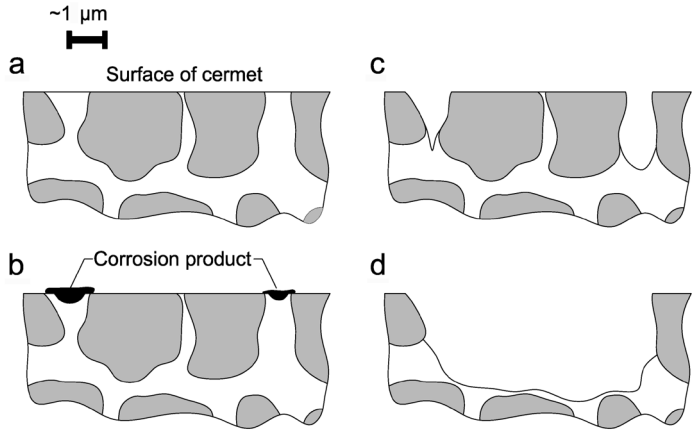

Fig. 10. Schematic representation of the cermet material degradation during the combined erosion-corrosion process. Dark phases indicate grains.

interaction and generally cannot be noticeably larger than the binder islands. Some islands can join each other but this is possible only if they are divided by small carbide grains.

A schematic representation of cermet material degradation is presented in Fig. 10 and described as follows.

A. Surface of the cermet before the erosion-corrosion process.

B. Corrosion starts in the centre of the largest binder island. Due to the good adhesion to the binder the corrosion island is growing while it reaches the carbide grains.

C. Corrosion products are removed by the action of the slurry solution and the interface between the matrix of the carbide grains is weakened. Once the interface is weakened, the particles of Cr_3C_2 are easily removed.
D. Several grains of the cermet are removed as a consequence of the combined erosion-corrosion effect.

Clearly the results show that the erosion-corrosion behaviour is very much dependent on the interaction between binder content, electrochemical potential and solution chemistry. Further investigations should elucidate the effect of particle concentration on the erosion-corrosion process in order to assess how the concentration of particles changes the erosion-corrosion mechanism of such materials.

4. CONCLUSIONS

1. The mechanism of Cr_3C_2-Ni wastage was investigated with the help of SEM micrographs and on the basis of numerical data obtained. The high erosion-corrosion resistance of the cermet with 10 wt % of Ni could be explained by the protective effect of the corrosion product.
2. Corrosion potential of chromium carbide based cermets with Ni binder has low tolerance to the change in binder concentration or the effect of abrasive particles.
3. A methodology for testing and evaluation of the erosion-corrosion parameters was applied and maps with defined wastage, regime, additive and synergistic regimes were constructed.

ACKNOWLEDGEMENTS

The authors are very grateful to the members of Tribology group of Strathclyde University, Glasgow, for help in organizing the experiments and constructive discussions of the work. Special acknowledgements are given to Kristjan Jaak Foundation, Estonia, for help in providing the financial support. The authors express their thanks to Dr. J. Pirso for supplying us with the test specimens. The work was carried out under a grant of the Estonian Science Foundation (grant No. 6163).

REFERENCES

1. Uusitalo, M., Vuoristo, T. and Mäntylä, T. Elevated erosion-corrosion in chlorine containing environments. *Wear*, 2002, **252**, 586–594.
2. Klimenko, V. and Masljuk, V. Corrosion resistant metalloceramic alloys on the base of chromium carbide. *Tekhnologiya i organizatsiya proizvodstva*, 1970, **3**, 82–85 (in Russian).
3. Lin, C. C., Lee, J. W., Chang, K. L., Hsieh, W. J., Wang, C. Y., Chang, Y. S. and Shih, H. C. The effect of the substrate bias voltage on the mechanical and corrosion properties of

chromium carbide thin film by filtered cathodic vacuum arc deposition. *Surf. Coat. Technol.*, 2005. Forthcoming.
4. Frangini, S., Masci, A. and Bartolomeo, A. D. Cr_7C_3-based cermet coating deposited on stainless steel by electrospark process: structural characteristics and corrosion behaviour. *Surf. Coat. Technol.*, 2002, **149**, 279–286.
5. Stack, M. M. and Pungwiwat, N. Erosion-corrosion mapping of Fe in aqueous slurries: some views on a new rationale for defining the erosion-corrosion interaction. *Wear*, 2004, **256**, 565–576.
6. Watson, S. W., Friedersdorf, F. J., Madsen, B. W. and Cramer, S. D. Methods of measuring wear-corrosion synergism. *Wear*, 1995, **181–183**, 476–484.
7. Ashby, M. F. *Materials Selection in Mechanical Design*. Butterworth-Heinemann, Oxford, 1992.
8. Stack, M. M. Mapping tribo-corrosion processes in dry and in aqueous conditions: some new directions for the new millennium. *Tribol. Internat.*, 2002, **35**, 681–689.
9. Sundararajan, G. and Roy, M. Solid particle erosion behaviour of metallic materials at room and elevated temperatures. *Tribol. Internat.*, 1997, **30**, 339–359.
10. Zu, J. B., Hutchings, I. M. and Burstein, G. T. Design of a slurry erosion test rig. *Wear*, 1990, **140**, 331–344.
11. Yue, Z., Zhou, P. and Shi, J. Some factors influencing corrosion-erosion performance of materials. In *Proc. Conference of Wear of Materials*. ASME, New York, 1987, 763–768.
12. Wright, I. G. Is there any reason to continue research efforts on erosion-corrosion? In *Proc. John Stringer Symposium on High Temperature Corrosion*. Ohio, 2001 (Tortorelli, P. F., Wright, I. G. and Hou, P. Y., eds.). ASM International, 2003, 107–121.
13. Craig, B. D. *Fundamental Aspects of Corrosion Films in Corrosion Science*. Plenum Press, New York, 1990.

Cr_3C_2-Ni-kermiste erosioon-korrosioon merevees

Maksim Antonov, Margaret Stack ja Irina Hussainova

Kroomkarbiidi baasil kermised pakuvad erinevates tööstusvaldkondades huvi unikaalsete omaduste tõttu. Nendel materjalidel on erosioonile märkimisväärne vastupanu temperatuuril kuni 1000 °C ja suurepärane oksüdeerimiskindlus kuni 850 °C. Nende korrosioonikindlus paljudes keskkondades on tunduvalt parem kui laialdaselt kasutatavatel WC-kermistel või roostevabadel terastel. Neid materjale võib kasutada ka pinnetena. On määratud prevaleerivad erosiooni- ja korrosiooni-protsessi režiimid ja koostatud erosiooni-korrosioonidiagrammid materjalide valikuks. Kroomkarbiidkermiste massi kadu samaaegsel erosioonil-korrosioonil on komplitseeritud ja seda ei saa vaadelda nende protsesside summana. SEM-meetodil on läbi viidud materjali pinna uuring enne ning pärast erosiooni-korrosioonikatset ja on määratud materjali käitumise prevaleerivad mehhanismid.